SUPPORTING INFORMATION

Gold nanoparticle size and shape effects on cellular uptake and intracellular distribution of siRNA nanoconstructs

Jun Yue,[†] Timothy Joel Feliciano,[†] Wenlong Li,[§] Andrew Lee,[#] and Teri W. Odom[†‡]*

[†]Department of Chemistry, [#]Department of Chemical and Biological Engineering, and [‡]Department of Materials Science and Engineering, Northwestern University, Evanston, Illinois 60208, United States

[§]School of Materials Science and Engineering, Nanyang Technological University, 639798, Singapore

[*]Corresponding author: todom@northwestern.edu

EXPERIMENTAL PROCEDURES S2
S1. Determination of AuNS surface area S2
S2. Cell uptake comparison of NP-siRNA vs. NP-siRNA/Cy5 ..... S3
Figure S1. Calibration curve of FITC-PEG loading vs. surface areas of AuNPs. S4
Figure S2. Pre-treatment with polyinosinic acid (poly(I)) led to decrease in the cellular uptake S5
Figure S3. Cellular uptake of NP-siRNA vs. NP-siRNA/Cy5 ..... S6
Figure S4. Confocal fluorescence images of U87 cells treated with NP-siRNA/Cy5 ..... S7
Figure S5. TEM images of cellular distribution of NP-siRNA constructs in U87 cells. S8
Table S1. Surface compositions of siRNA-NP constructs for cell uptake comparison S9
Table S2. Surface compositions of Cy5-labeled AuNPs for confocal microscopy imaging S10
Table S3. Summary of subcellular locations of gold nanoparticles by TEM in publications S11

EXPERIMENTAL PROCEDURES

S1. Determination of AuNS surface area

The surface area of AuNS was determined from a series of spherical NPs with the hypothesis that the loading capacity of thiolated molecules on AuNS equals to that on a spherical AuNP if they have the same surface area. Because the surface area of spherical AuNP with specific size is known, we firstly determined the loading capacity of FITC-labeled PEG-SH (Nanocs. Cat. No. PG2-FCTH-2k) on a series of spherical AuNPs (5 nm, 10 nm, 20 nm, 30 nm, 40 nm, 50 nm, 60 nm, and 80 nm) to obtain the calibration curve of loading capacity as a function of surface area (Figure S1). To realize the maximum loading of PEG on each AuNP, excess of PEG molecules (13 PEG per nm^2) were incubated with the AuNP solution in Millipore water at room temperatures for 5 h, followed by multiple centrifugations to remove the excess of PEG until the supernatant has no detectable fluorescence. The AuNP pellet was digested in 100 mM of KCN to determine the fluorescent intensity of FITC (FI_{FITC}) and thus the loading of PEG on each AuNP was calculated from the calibration curve of FI_{FITC} *vs.* PEG concentration. Next, we conjugated the AuNS with PEG using the molar ratio of 100000/1 (PEG/AuNS). Using the same conditions, the loading of PEG on AuNS was determined. Finally, according to the calibration curve of loading capacity *vs.* surface area, we found the surface area of AuNS (7790 nm^2) is close to 50 nm spherical NP (7840 nm^2).

S2. Cell uptake comparison of NP-siRNA *vs.* NP-siRNA/Cy5

U87 cells were plated on 12-well plates with the density of 2×10^4 cells / well and cultured in complete growth media at 37 ^oC with 5% CO_2 for 24 h. Then cells were treated with 0.5 nM of NP-siRNA or NP-siRNA/Cy5 nanoconstructs for a prescribed time (2 h and 24 h). At each time point, the supernatant was removed and cells were washed 3 times with PBS, followed by trypsinization to isolate the cells from the plates. The isolated cells were transferred to a 1.5 mL of Eppendorf tube and washed 3 times with PBS by centrifugation at 300 *g* × 5 min. After washing, cell pellets were resuspended in PBS and cell numbers were counted using a hemocytometer. Finally, cells were lysed in acid solution (2% HCl + 2% HNO3) at 70 ^oC overnight for gold quantifications by inductively coupled plasma mass spectrometry (ICP-MS).

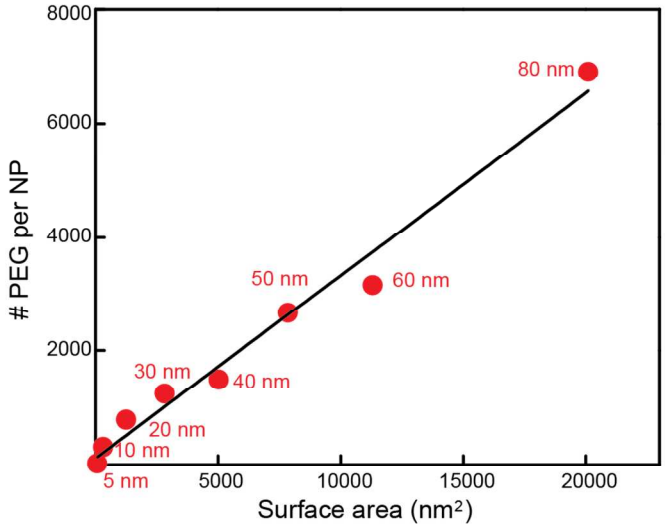

Figure S1. Calibration curve of FITC-PEG loading vs. surface areas of AuNPs.

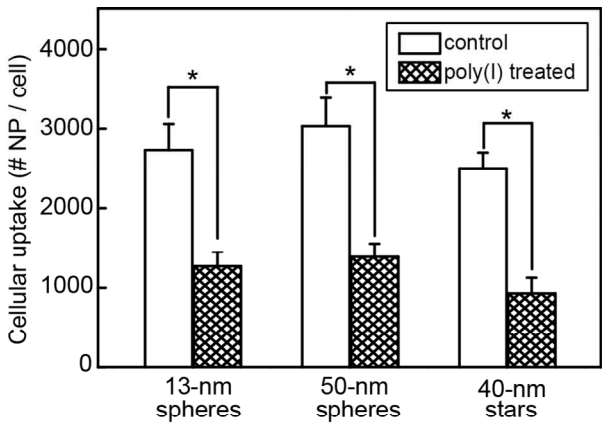

Figure S2. Pre-treatment with polyinosinic acid (poly(I)) led to a decrease in cellular uptake of NP-siRNA constructs by U87 cells. Following a 30-min pre-treatment with 10 μg/mL of poly(I), U87 cells were incubated with NP-siRNA (0.5 nM in NP) in poly(I) for 2 h and cell uptake was then measured by ICP-MS. As a control, U87 cells were also treated with constructs under the same conditions but without poly(I), $*p < 0.05$.

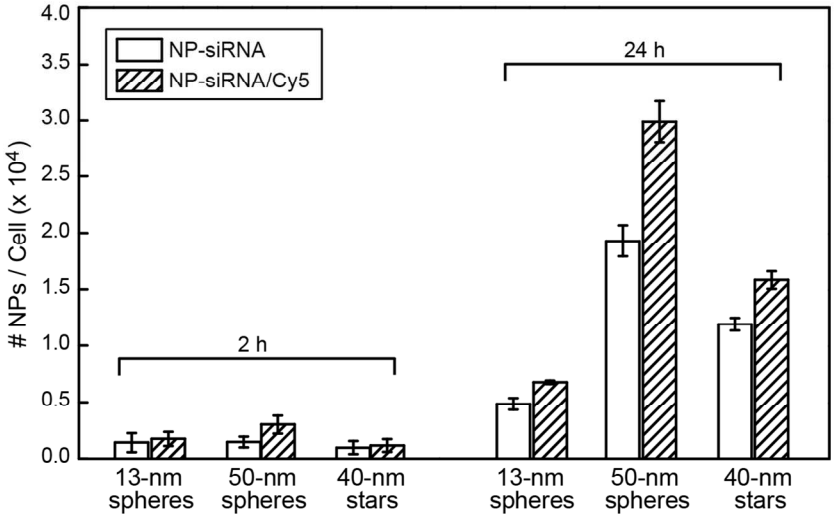

Figure S3. Cellular uptake of NP-siRNA *vs.* NP-siRNA/Cy5 for each formulation at two representative time points (2 h and 24 h).

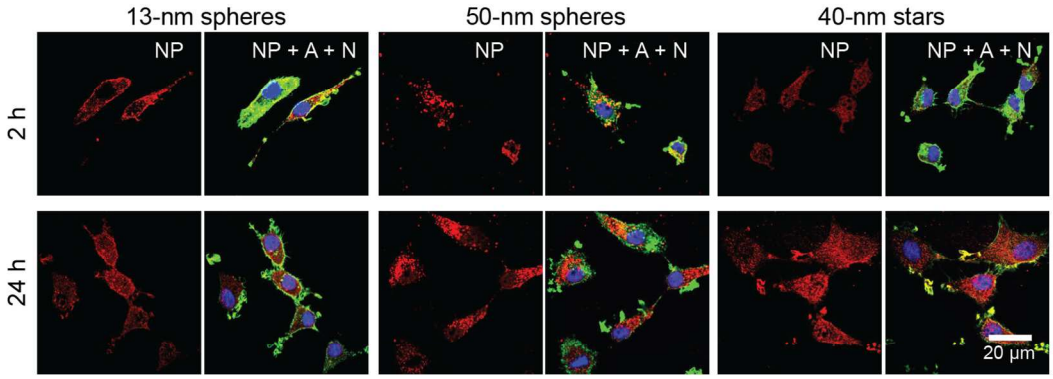

Figure S4. Confocal fluorescence images of U87 cells treated with NP-siRNA/Cy5 constructs with the equivalent concentration of RNA strands and dT20-Cy5 for 2 h and 24 h.

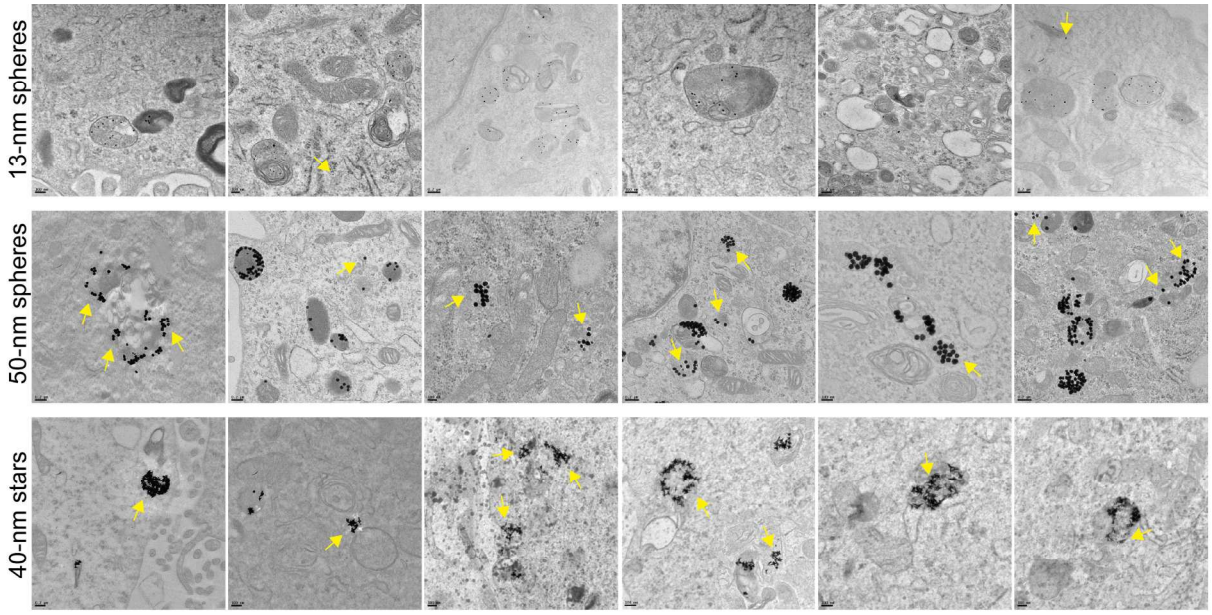

Figure S5. TEM images of cellular distribution of NP-siRNA constructs in U87 cells. Cells were treated with 0.5 nM of 13-nm spheres, 50-nm spheres, or 40-nm stars for 24 h. Yellow arrows indicate NPs distributed outside of vesicle structures.

Table S1. Surface compositions of siRNA-NP constructs for cell uptake comparison

Core	Surface area (nm^2)	Size effect				Shape effect			
		#(S+AS) / NP	#(S+AS) / nm^2	#AS / NP	#AS / nm^2	#(S+AS) / NP	#(S+AS) / nm^2	#AS / NP	#AS / nm^2
13-nm spheres	531	83	0.156	23	0.043	N/A	N/A	N/A	N/A
50-nm spheres	7840	1291	0.165	329	0.042	1001	0.128	221	0.028
40-nm stars	7790	N/A	N/A	N/A	N/A	1023	0.131	251	0.032

N/A: not available; S and AS represents sense and anti-sense strands respectively

Table S2. Surface compositions of Cy5-labeled AuNPs for confocal microscopy imaging

Core	dT_{20}-Cy5 (molecules / NP)	AS (molecules / NP)	S (molecules / NP)	Density of RNA (molecules nm^{-2})
13-nm spheres	6 ± 2	21 ± 5	86 ± 8	0.21
50-nm spheres	56 ± 6	259 ± 62	1168 ± 52	0.19
40-nm stars	54 ± 4	262 ± 34	1056 ± 54	0.18

S and AS represents sense and anti-sense strands, respectively.

Table S3. Summary of subcellular locations of gold nanoparticles by TEM in publications

AuNP core	surface ligands	subcellular location	cell line	incubation time	Ref. #
spheres (5, 10, 20, 40 nm)	citrate	vesicles	SGC-7901 HepG2	24 h 2-24 h	1, 2
spheres (2-3, 10 nm)	phospho-lipid	vesicles	HeLa	2 h	3
spheres (18, 35, 65 nm)	HPMA polymer	vesicles	hCMEC/D3 HDMEC	24 h	4
nanorods	RGD	cytoplasm	A375	1 h	5
spheres (2-6, 15 nm)	drug tiopronin	nucleus, cytoplasm (2–6 nm); cytoplasm (15-nm)	MCF-7	24 h	6
nanostars (25 nm)	AS1411	vesicles, cytoplasm (perinuclear regions)	HeLa, HT-1080, PANC-1	0-72 h	7, 8
nanostars (40 nm)	HER2 aptamer	lysosomes	SK-BR-3	24 h	9
spheres (13, 50 nm); stars (40 nm)	siRNA	vesicles (13-nm spheres); vesicles, cytoplasm (50-nm spheres and 40-nm stars)	U87	24 h	current study

SGC-7901: human gastric cancer cell line; HepG2: HepG2: human hepatoma carcinoma cells; HeLa: human cervical cancer cells; hCMEC/D3: blood-brain barrier cell line; HDMEC: primary human dermal microvascular endothelial cells; A375: human melanoma cell line; MCF-7: human breast cancer cells; HT-1080: human fibrosarcoma; PANC-1: human pancreatic cancer cell line; SK-BR-3: human breast cancer cell line; U87: human glioblastoma cell line; HPMA: *N*-(2-Hydroxypropyl) methacrylamide; RGD: Arg-Gly-Asp tripeptide; AS1411: anti-nucleolin aptamer; HER2: human epidermal growth factor receptor 2.

(1) Wu, Y., Zhang, Q., Ruan, Z., and Yin, Y. (2016) Intrinsic effects of gold nanoparticles on proliferation and invasion activity in SGC-7901 cells. *Oncol Rep 35*, 1457-62.

(2) Lu, P., Wang, J., Lin, J., Lin, J., Liu, N., Huang, Z., Li, B., Zeng, H., and Chen, R. (2015) Gold nanoaggregates for probing single-living cell based on surface-enhanced Raman spectroscopy. *J Biomed Opt 20*, 051005.

(3) Gordillo, G. J., Krpetic, Z., and Brust, M. (2014) Interactions of gold nanoparticles with a phospholipid monolayer membrane on mercury. *ACS Nano 8*, 6074-80.

(4) Freese, C., Unger, R. E., Deller, R. C., Gibson, M. I., Brochhausen, C., Klok, H. A., and Kirkpatrick, C. J. (2013) Uptake of poly(2-hydroxypropylmethacrylamide)-coated gold nanoparticles in microvascular endothelial cells and transport across the blood-brain barrier. *Biomater Sci-Uk 1*, 824-833.

(5) Xu, W., Luo, T., Li, P., Zhou, C., Cui, D., Pang, B., Ren, Q., and Fu, S. (2012) RGD-conjugated gold nanorods induce radiosensitization in melanoma cancer cells by downregulating alpha(v)beta(3) expression. *Int J Nanomedicine 7*, 915-24.

(6) Huang, K., Ma, H., Liu, J., Huo, S., Kumar, A., Wei, T., Zhang, X., Jin, S., Gan, Y., Wang, P. C., et al. (2012) Size-dependent localization and penetration of ultrasmall gold nanoparticles in cancer cells, multicellular spheroids, and tumors in vivo. *ACS Nano 6*, 4483-93.
(7) Dam, D. H., Lee, J. H., Sisco, P. N., Co, D. T., Zhang, M., Wasielewski, M. R., and Odom, T. W. (2012) Direct observation of nanoparticle-cancer cell nucleus interactions. *ACS Nano 6*, 3318-26.
(8) Dam, D. H., Lee, R. C., and Odom, T. W. (2014) Improved in vitro efficacy of gold nanoconstructs by increased loading of G-quadruplex aptamer. *Nano Lett 14*, 2843-8.
(9) Lee, H., Dam, D. H., Ha, J. W., Yue, J., and Odom, T. W. (2015) Enhanced Human Epidermal Growth Factor Receptor 2 Degradation in Breast Cancer Cells by Lysosome-Targeting Gold Nanoconstructs. *ACS Nano 9*, 9859-67.